Metal–Organic Frameworks

DOI: 10.1002/anie.201001009

An Isoreticular Series of Metal–Organic Frameworks with Dendritic Hexacarboxylate Ligands and Exceptionally High Gas-Uptake Capacity**

*Daqiang Yuan, Dan Zhao, Daofeng Sun, and Hong-Cai Zhou**

Metal–organic frameworks (MOFs) are newly emerging porous materials.[1] Owing to their large surface area and tunable pore size and geometry, they have been studied for applications in gas storage and separation, especially in hydrogen and methane storage and carbon dioxide capture.[2] It has been well established that the high-pressure gravimetric hydrogen-adsorption capacity of an MOF is directly proportional to its surface area.[3] However, MOFs of high surface areas tend to decompose upon activation. In our previous work, we described an approach toward stable MOFs with high surface areas by incorporating mesocavities with microwindows.[4] To extend this work, we now present an isoreticular[5] series of (3,24)-connected MOFs made from dendritic hexacarboxylate ligands, one of which has a Langmuir surface area as high as 6033 $m^2 g^{-1}$. In addition, the gas-adsorption properties of this new isoreticular MOF series have been studied.

To construct the (3,24)-connected isoreticular MOF series, the ligands should have C_3 symmetry with three coplanar isophthalate moieties.[4] Bearing this in mind, we designed and synthesized two dendritic hexacarboxylic acids: H_6ptei and H_6ttei (Figure 1a). The ensuing solvothermal reactions between these carboxylic acids and copper salts led to two isostructural MOFs with the same (3,24)-connected network (Figure 1b), designated PCN-68 $(Cu_3(H_2O)_3$-(ptei)·13 H_2O·33 dmf) and PCN-610 $(Cu_3(H_2O)_3$-(ttei)·19 H_2O·22 dmf) (PCN stands for porous coordination network). Together with PCN-61 and PCN-66,[4] four MOFs form a new isoreticular MOF series. As reported previously, the structure of these MOFs can be described as the packing of three types of polyhedra: cuboctahedra (cubOh, red), truncated tetrahedra (T-Td, green), and truncated octahedra (T-Oh, blue; Figure 1c). The diameters of spheres representing the void inside these polyhedra are listed in Table 1. As expected, the ligand extension has enlarged the size of T-Oh, which is accompanied by a mild increase in the size of T-Td, and no change in the size of cubOh. It is evident that the pore size of T-Oh has reached the meso range in PCN-66, PCN-68, and PCN-610.

Calculations and experimental evidence support the assessment that given fixed framework topology, the surface

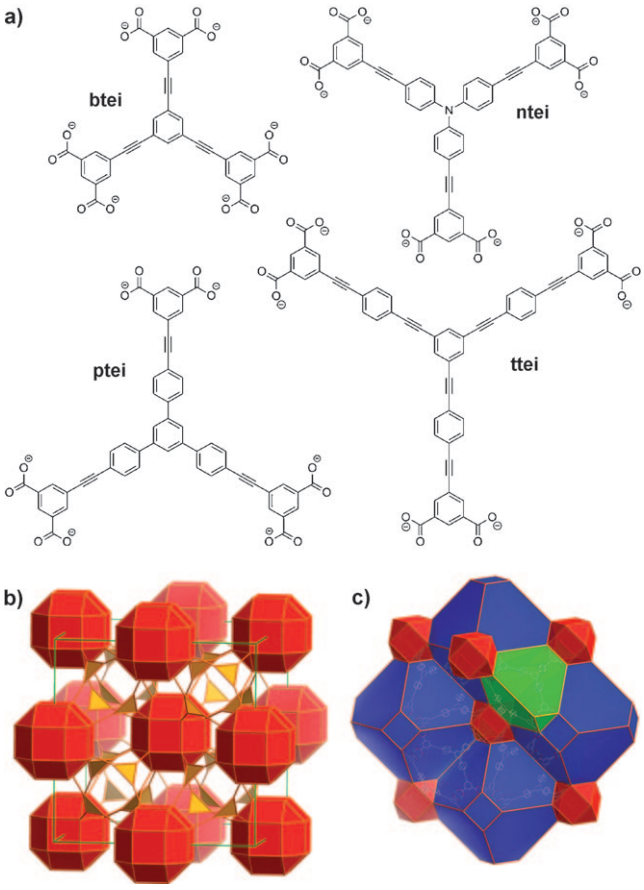

Figure 1. a) Nanoscopic ligands btei (PCN-61), ntei (PCN-66), ptei (PCN-68), and ttei (PCN-610); b) (3,24)-connected network in PCN-68; c) 3D polyhedra packing in PCN-68.

[*] Dr. D. Yuan,[+] D. Zhao,[+] Prof. Dr. H.-C. Zhou
Department of Chemistry, Texas A&M University
College Station, TX 77843 (USA)
Fax: (+1) 979-845-1595
E-mail: zhou@mail.chem.tamu.edu
Homepage: http://www.chem.tamu.edu/rgroup/zhou/
Prof. Dr. D. Sun
Key Lab for Colloid and Interface Chemistry
Shandong University, Jinan (P.R. China)
[+] These authors contributed equally to this work.

[**] This work was supported by the US Department of Energy (DE-FC36-07GO17033) and the Welch Foundation (A-1725). The microcrystal diffractions of PCN-68 and PCN-610 were carried out with the assistance of Yu-Sheng Chen at the Advanced Photon Source on beam line 15ID-B at ChemMatCARS Sector 15, which is principally supported by the National Science Foundation/Department of Energy under grant number CHE-0535644. Use of the Advanced Photon Source was supported by the US Department of Energy, Office of Science, Office of Basic Energy Sciences, under Contract No. DE-AC02-06CH11357.

Supporting information for this article is available on the WWW under http://dx.doi.org/10.1002/anie.201001009.

Table 1: Unit cell length ($Fm\bar{3}m$), ligand size (L size), and polyhedron size of the isoreticular PCN-6X MOF series.

Material	Unit cell length [Å]	L size [Å][a]	CubOh size [Å]	T-Td size [Å]	T-Oh size [Å]
PCN-61	42.796	6.906	12.0	11.8	18.8
PCN-66	49.112	9.758	12.0	12.0	20.6
PCN-68	52.738	11.243	12.0	14.8	23.2
PCN-610	59.153	13.815	12.0	18.6	26.0

[a] The ligand size is defined as the distance between the center of the ligand and the center of a terminal benzene ring.

Table 2: Surface areas, pore volumes, and porosities of the isoreticular PCN-6X MOFs.

Material	Surface area [$m^2 g^{-1}$] (Langmuir/BET/calcd[a])	Pore volume [$cm^3 g^{-1}$] (exptl/calcd[a])	Porosity[a]
PCN-61	3500/3000/3455	1.36/1.37	77.0%
PCN-66	4600/4000/3746	1.63/1.75	80.0%
PCN-68	6033/5109/3871	2.13/2.17	82.9%
PCN-610[b]	NA/NA/4160	NA/3.00	86.8%

[a] Calculated using Material Studio 4.4. [b] NA = not available.

area of a framework increases with ligand extension in all currently explored systems.[6] In reality, however, frameworks built with long spacers tend to collapse after the removal of guest molecules.[7] In addition, longer ligands may cause framework interpenetration, resulting in a reduced surface area or even a nonporous structure.[8] In the (3,24)-connected network, the commonly encountered framework instability accompanying ligand extension can be alleviated by using dendritic ligands.[4] The isophthalate moiety of the ligand produces cubOh with a fixed size, limiting the open window sizes of the T-Td and T-Oh, although the sizes of the T-Td and T-Oh will expand with the ligand extension. Thus, by using ligands longer than those in PCN-61 and PCN-66, stable MOFs with surface areas higher than those found in PCN-61 and PCN-66 can be made. This hypothesis will be examined in PCN-68 and PCN-610.

To test the framework stability, nitrogen sorption measurements were carried out in fully activated PCN-68 and PCN-610. In PCN-68, a dramatic increase of nitrogen sorption was observed (Figure 2). The BET surface area calculated on

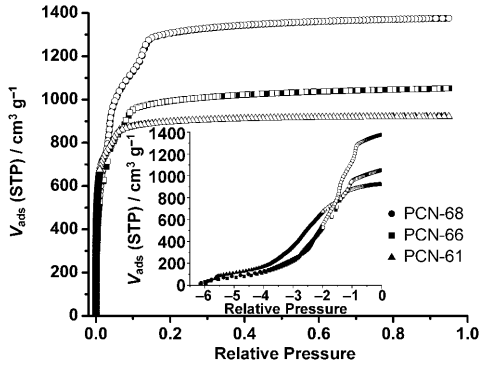

Figure 2. N_2 sorption isotherms of PCN-61, PCN-66, and PCN-68 at 77 K.

the basis of the low-pressure region data can reach as high as 5109 $m^2 g^{-1}$, and the Langmuir surface area as high as 6033 $m^2 g^{-1}$. To the best of our knowledge, PCN-68 possesses the highest surface area reported to date for MOFs based on paddlewheel clusters, and it is also among the highest reported (Table 2).[6a,9] The pore size data calculated on the basis of nitrogen sorption isotherms are consistent with the crystal data (Figure S1 in the Supporting Information). Careful examination of the low-pressure region reveals stepwise sorption behavior, which is typical for materials with hierarchical pore size distribution.[4] However, with PCN-610, in which an even larger ligand was used, there is barely any nitrogen sorption observed, implying a complete collapse of the framework. The same conclusion is also drawn from the powder X-ray diffraction (PXRD) data, which reveal that PCN-610 lost its crystallinity completely upon activation (Figure S2 in the Supporting Information).

From the above discussion, it is evident that by using the dendritic hexacarboxylate ligands, isoreticular MOFs with higher surface areas can be obtained by ligand extension. However, this approach, which is based on the formation of cuboctahedra and a (3,24)-connected framework, has its limitations. The ligand size that may lead to a stable MOF with the highest surface areas in this series falls between ptei (11.2 Å) in PCN-68 and ttei (13.8 Å) in PCN-610. In addition, the (3,24)-connected network can incorporate ligands as large as 11.2 Å without framework decomposition, whereas in the twisted boracite network, which is composed of tricarboxylate ligands (less dendritic) and dimetal paddlewheels,[10] even a ligand as small as 4.179 Å (tatb, 4,4′,4″-*s*-triazine-2,4,6-triyl-tribenzoate) would lead to the disintegration of the PCN-6′ framework.[10c] It is our belief that dendritic ligands with more branches will lead to stable MOFs that can tolerate more extended ligands, leading to even higher surface areas.[11]

The high surface areas of the isoreticular PCN-6X series of PCN-61, PCN-66, and PCN-68 prompted us to study their gas-uptake capacity, especially that for hydrogen, methane, and carbon dioxide.[2] Hydrogen is an ideal energy carrier. However, the lack of an effective storage method hinders its application. The US Department of Energy (DOE) recently reset the gravimetric and volumetric storage targets for on-board hydrogen storage for the year 2010 (4.5 wt%, 28 $g L^{-1}$) and 2015 (5.5 wt%, 40 $g L^{-1}$).[12] MOF-based hydrogen storage has attracted remarkable attention recently because of its fast kinetics and favorable thermodynamics in hydrogen adsorption and release.[3,9b,13] The hydrogen-uptake capacities of PCN-6X series are shown in Figure 3. In the low-pressure region (< 1 bar), the hydrogen-uptake capacity is mainly controlled by the hydrogen affinity towards the framework, which can be quantified by the isosteric heat of adsorption (Figure S3 in the Supporting Information). PCN-61, which has the smallest pore size, also has the highest heat of adsorption and highest capacity (2.25 wt% at 77 K, 1 bar). PCN-66 and PCN-68 have heats of adsorption and adsorption capacities similar to each other (1.79 wt% in PCN-66 vs. 1.87 wt% in PCN-68). This trend is consistent with the nature

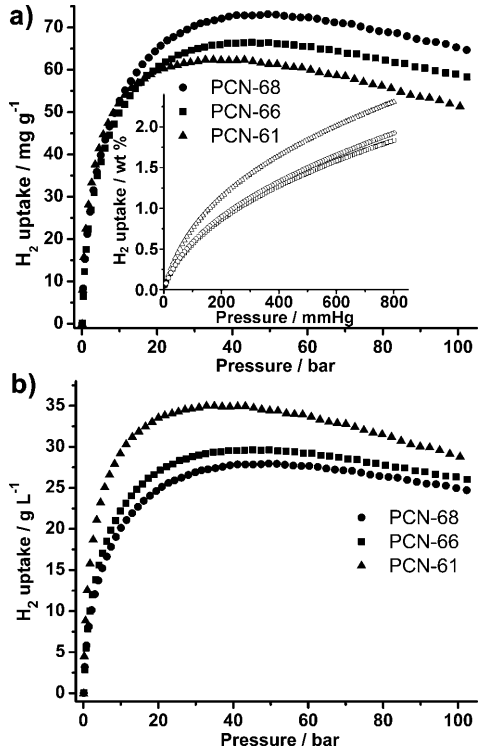

Figure 3. a) Gravimetric and b) volumetric H_2-uptake in PCN-6X series at 77 K. The inset in (a) shows the low-pressure region enlarged.

of physisorption, in which narrower pores would have stronger interactions with the guest gas molecules because of the increased interaction between the guests and the opposite potential walls within small pores.[14]

Unlike the low-pressure hydrogen sorption capacity, which is dominated by the hydrogen affinity, the maximum excess hydrogen-uptake capacity in MOFs, which typically can only be reached in the high-pressure range, is controlled mainly by the surface area and pore volume.[3,15] This behavior is consistent with what has been observed in the PCN-6X series. As can be seen from Figure 3a, PCN-68, which has the highest surface area, also has the highest maximum excess hydrogen-uptake capacity (73.2 mg g^{-1}, Table 3). Its hydrogen-uptake capacity is comparable with that of the current record holder, MOF-177 (75 mg g^{-1}).[16] Taking into consideration the gaseous hydrogen compressed within the framework void, its total hydrogen-uptake capacity would reach 130 mg g^{-1} (100 bar) (Figure S4 in the Supporting Information), which makes it one of the best adsorbents with the highest gravimetric hydrogen-uptake capacity.[2] It is worth noting that the maximum adsorption pressure increases from PCN-61 (33 bar) to PCN-66 (45 bar) and PCN-68 (50 bar), indicating higher pressure is needed to reach maximum adsorption in sorbents with higher pore volumes.

Using the crystal-density data, the volumetric hydrogen-uptake capacities were also calculated (Figure 3b). Unlike the trend in gravimetric capacity, in which the material with the highest surface area has the highest capacity, the volumetric capacity follows the opposite trend, which is dominated by the densities of the sorbents. The gravimetric capacity has been emphasized in past hydrogen-storage research, and rightfully so. However, the volumetric capacity is particularly relevant in volume-limited fuel-cell applications.[17] Both of these criteria should be emphasized equally in the search for ideal hydrogen-storage materials.

Natural gas (methane being the main component) is another alternative on-board fuel that has aroused much interest. Like hydrogen, however, it also lacks an effective storage method. The DOE target for on-board methane storage is based on volumetric capacity (180 v(STP)/v(STP) under 35 bar and near ambient temperature; STP = standard temperature and pressure; $T = 273.15$ K, $P = 101.325$ kPa), which requires the adsorbents to have not only high porosity, but also high packing density and good thermal conductivity.[18] PCN-6X series MOFs have been tested for their methane-uptake capacities at 298 K. As can be seen from Figure 4a, the gravimetric methane-uptake capacities in these

Table 3: Hydrogen-uptake capacities and isosteric heats of adsorption in the PCN-6X series.

Material	H_2 uptake at 77 K, 1 atm [wt%] (g L^{-1})[a]	Maximum excess H_2 uptake [mg g^{-1}] (g L^{-1})[a]	Q_{ST} [kJ mol^{-1}]
PCN-61	2.25 (12.6)	62.4 (35.0) 33 bar 77 K 6.67 (3.74) 90 bar 298 K	6.36
PCN-66	1.79 (7.98)	66.5 (29.6) 45 bar 77 K 7.85 (3.50) 90 bar 298 K	6.22
PCN-68	1.87 (7.20)	73.2 (28.0) 50 bar 77 K 10.1 (4.10) 90 bar 298 K	6.09

[a] The values in parentheses represent the volumetric hydrogen-uptake capacities.

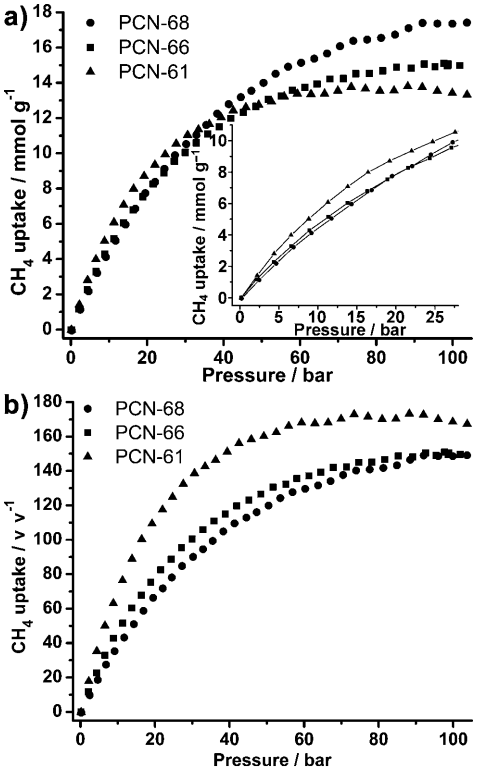

Figure 4. a) Gravimetric and b) volumetric capacities of CH_4 adsorption in the PCN-6X series at 298 K. The inset in (a) shows the medium-pressure region enlarged.

MOFs are also proportional to their surface areas. In the medium-pressure range (< 20 bar), PCN-61 has the highest capacity, possibly because of the stronger methane affinity of the framework, which can be ascribed to the small pore size. When the pressure goes to high range (> 60 bar), the effect of surface area and pore volume starts to dominate, making PCN-68 the one with the highest uptake. By assuming the crystal density as the packing density, the volumetric methane-uptake capacities were also calculated (Figure 4b). PCN-61 has the highest capacity at 35 bar (145 v/v), followed by PCN-66 (110 v/v), and PCN-68 (99 v/v) (Table 4). This trend can be ascribed to the difference in crystal density among the three structures (0.56 $g\,cm^{-3}$ in PCN-61 vs. 0.45 $g\,cm^{-3}$ in PCN-66 and 0.38 $g\,cm^{-3}$ in PCN-68). From this study, it can be concluded that high surface area should not be the sole emphasis if the aim is to achieve high volumetric methane-uptake capacity. Instead, a balance should be maintained among porosity, density, pore size, and other factors.

Table 4: CH_4 and CO_2 excess uptake capacities in the PCN-6X series at 35 bar and 298 K.

Material	CH_4 [mmol g^{-1}]	CH_4 [v v^{-1}]	CO_2 [mmol g^{-1}]
PCN-61	11.6	145	23.5
PCN-66	11.1	110	26.3
PCN-68	11.6	99	30.4

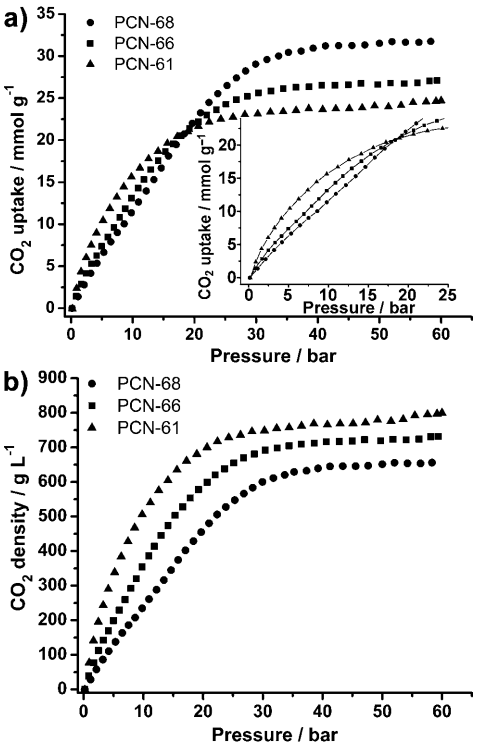

Figure 5. Gravimetric CO_2 uptake (a) and density (b) in the PCN-6X series at 298 K.

Aggravated global warming, which is partially attributed to the increasing carbon dioxide concentration in the air, has aroused worldwide concerns. Carbon capture and sequestration (CCS), a process involving the capture of carbon dioxide from the air and sequestering it underground, has been proposed as a feasible way to control the atmospheric carbon dioxide concentration.[19] Using porous materials to capture carbon dioxide based on the sorption mechanism will be an energy-conserving alternative approach. The study of MOF-based carbon dioxide capture is growing dramatically.[2] The high-pressure gravimetric carbon dioxide adsorption capacities of the PCN-6X series at 298 K are shown in Figure 5a. Once again, their storage capacities follow a trend similar to those found in the aforementioned hydrogen- and methane-adsorption studies. PCN-68 has the highest gravimetric carbon dioxide storage capacity among the three frameworks, and is also among the highest reported (Table 4). The density of the carbon dioxide captured can be calculated on the basis of the amount of gas adsorbed and the pore volume of the frameworks (Figure 5b). The density of adsorbed carbon dioxide is the highest in PCN-61. Based on the total capacity, at 35 bar and room temperature, a container filled with PCN-61 can store 8.2 times the amount of CO_2 in an empty container, and this volumetric capacity is 7.3 for PCN-66 and 7.4 for PCN-68, which make PCN-6X series compounds good adsorbents for carbon dioxide capture.

In summary, an isoreticular MOF series with the (3,24)-connected network topology has been synthesized by using a series of dendritic hexacarboxylate ligands. The framework is stabilized by incorporating microwindows, whose size is fixed by the formation of cuboctahedra supported by the isophthalate moieties throughout the framework. The mesocavities, which are connected by the microwindows, however, are sustained by these nanoscopic ligands and responsible for the porosity improvement with ligand extension. In addition, the formation of isophthalate-sustained cuboctahedra in the (3,24)-connected network prohibits framework interpenetration, leading to MOFs with close to record-high surface areas. Hydrogen, methane, and carbon dioxide adsorption studies of MOFs in this series also revealed close to record-high gas-adsorption capacities. However, this approach has its limitations. The ligand size that may lead to a stable MOF with the highest surface areas in this isoreticular series falls between 11.2 and 13.8 Å. We propose that dendritic ligands with even more branches should lead to stable MOFs that can tolerate more extended ligands leading to even higher surface areas. Work along those lines is currently underway in our laboratory.

Experimental Section

Crystal data for PCN-68: $C_{54}H_{30}Cu_3O_{15}$, $M = 1109.40$, green prism, $0.03 \times 0.02 \times 0.02$ mm^3, cubic, space group $Fm\bar{3}m$, $a = 52.738(5)$, $V = 146679(24)$ $Å^3$, $Z = 32$, $\rho_{calcd} = 0.402$ $g\,cm^{-3}$, $F_{000} = 17952$, synchrotron radiation, $\lambda = 0.41328$ Å, $T = 173(2)$ K, $2\theta_{max} = 23.9°$, 389054 reflections collected, 3753 unique ($R_{int} = 0.2923$). Final GooF = 1.429, $R_1 = 0.1556$, $wR_2 = 0.3923$, R indices based on 2340 reflections with $I > 2\sigma(I)$, $\mu = 0.193$ mm^{-1}.

Crystal data for PCN-610: $C_{60}H_{30}Cu_3O_{15}$, $M = 1181.46$, green prism, $0.03 \times 0.02 \times 0.02$ mm^3, cubic, space group $Fm\bar{3}m$, $a = 59.153(6)$, $V = 206977(39)$ $Å^3$, $Z = 32$, $\rho_{calcd} = 0.303$ $g\,cm^{-3}$, $F_{000} = 19104$, synchrotron radiation, $\lambda = 0.41328$ Å, $T = 150(2)$ K, $2\theta_{max} = 15.8°$,

189298 reflections collected, 1650 unique ($R_{int} = 0.2187$). Final GooF = 1.210, $R_1 = 0.1227$, $wR_2 = 0.3300$, R indices based on 1395 reflections with $I > 2\sigma(I)$, $\mu = 0.137$ mm^{-1}.

CCDC 764972 (PCN-68) and 764973 (PCN-610) contain the supplementary crystallographic data for this paper. These data can be obtained free of charge from The Cambridge Crystallographic Data Centre via www.ccdc.cam.ac.uk/data_request/cif.

Full experimental details are presented in the Supporting Information.

Received: February 17, 2010
Published online: June 11, 2010

Keywords: carbon storage · clean energy · hydrogen · metal–organic frameworks · methane

[1] S. Kitagawa, R. Kitaura, S. Noro, *Angew. Chem.* **2004**, *116*, 2388 – 2430; *Angew. Chem. Int. Ed.* **2004**, *43*, 2334 – 2375.
[2] S. Q. Ma, H. C. Zhou, *Chem. Commun.* **2010**, *46*, 44 – 53.
[3] D. Zhao, D. Q. Yuan, H. C. Zhou, *Energy Environ. Sci.* **2008**, *1*, 222 – 235.
[4] D. Zhao, D. Q. Yuan, D. F. Sun, H. C. Zhou, *J. Am. Chem. Soc.* **2009**, *131*, 9186 – 9188.
[5] O. M. Yaghi, M. O'Keeffe, N. W. Ockwig, H. K. Chae, M. Eddaoudi, J. Kim, *Nature* **2003**, *423*, 705 – 714.
[6] a) H. K. Chae, D. Y. Siberio-Pérez, J. Kim, Y. B. Go, M. Eddaoudi, A. J. Matzger, M. O'Keeffe, O. M. Yaghi, *Nature* **2004**, *427*, 523 – 527; b) K. S. Walton, R. Q. Snurr, *J. Am. Chem. Soc.* **2007**, *129*, 8552 – 8556; c) S. S. Han, W. A. Goddard, *J. Phys. Chem. C* **2008**, *112*, 13431 – 13436.
[7] A. P. Nelson, O. K. Farha, K. L. Mulfort, J. T. Hupp, *J. Am. Chem. Soc.* **2009**, *131*, 458 – 460.
[8] S. R. Batten, R. Robson, *Angew. Chem.* **1998**, *110*, 1558 – 1595; *Angew. Chem. Int. Ed.* **1998**, *37*, 1460 – 1494.
[9] a) G. Férey, C. Mellot-Draznieks, C. Serre, F. Millange, J. Dutour, S. Surblé, I. Margiolaki, *Science* **2005**, *309*, 2040 – 2042; b) K. Koh, A. G. Wong-Foy, A. J. Matzger, *J. Am. Chem. Soc.* **2009**, *131*, 4184 – 4185.
[10] a) S. S. Y. Chui, S. M. F. Lo, J. P. H. Charmant, A. G. Orpen, I. D. Williams, *Science* **1999**, *283*, 1148 – 1150; b) D. F. Sun, S. Q. Ma, Y. X. Ke, D. J. Collins, H. C. Zhou, *J. Am. Chem. Soc.* **2006**, *128*, 3896 – 3897; c) S. Q. Ma, D. F. Sun, M. Ambrogio, J. A. Fillinger, S. Parkin, H. C. Zhou, *J. Am. Chem. Soc.* **2007**, *129*, 1858 – 1859; d) X. S. Wang, S. Q. Ma, D. F. Sun, S. Parkin, H. C. Zhou, *J. Am. Chem. Soc.* **2006**, *128*, 16474 – 16475.
[11] L. Q. Ma, D. J. Mihalcik, W. B. Lin, *J. Am. Chem. Soc.* **2009**, *131*, 4610 – 4612.
[12] DOE Targets for On-Board Hydrogen Storage Systems for Light-Duty Vehicles, available at: http://www1.eere.energy.gov/hydrogenandfuelcells/storage/pdfs/targets_onboard_hydro_storage.pdf.
[13] a) N. L. Rosi, J. Eckert, M. Eddaoudi, D. T. Vodak, J. Kim, M. O'Keeffe, O. M. Yaghi, *Science* **2003**, *300*, 1127 – 1129; b) L. J. Murray, M. Dinca, J. R. Long, *Chem. Soc. Rev.* **2009**, *38*, 1294 – 1314; c) N. Klein, I. Senkovska, K. Gedrich, U. Stoeck, A. Henschel, U. Mueller, S. Kaskel, *Angew. Chem.* **2009**, *121*, 10139 – 10142; *Angew. Chem. Int. Ed.* **2009**, *48*, 9954 – 9957.
[14] P. Bénard, R. Chahine, *Scr. Mater.* **2007**, *56*, 803 – 808.
[15] H. Frost, T. Düren, R. Q. Snurr, *J. Phys. Chem. B* **2006**, *110*, 9565 – 9570.
[16] H. Furukawa, M. A. Miller, O. M. Yaghi, *J. Mater. Chem.* **2007**, *17*, 3197 – 3204.
[17] U. Mueller, M. Schubert, F. Teich, H. Puetter, K. Schierle-Arndt, J. Pastré, *J. Mater. Chem.* **2006**, *16*, 626 – 636.
[18] T. Düren, L. Sarkisov, O. M. Yaghi, R. Q. Snurr, *Langmuir* **2004**, *20*, 2683 – 2689.
[19] R. S. Haszeldine, *Science* **2009**, *325*, 1647 – 1652.

